Research Square

Preprints are preliminary reports that have not undergone peer review.
They should not be considered conclusive, used to inform clinical practice,
or referenced by the media as validated information.

Electronic structure, cationic and excited states of nitrogen-containing spiroborates

Andrey Sidorin (sae94@mail.ru)
Far Eastern Federal University
Sergey Tikhonov
Kamchatka Branch of the Geophysical Survey of the Russian Academy of Sciences
Ilya Samoilov
Saint Petersburg State University
Ivan Osmushko
Far Eastern Federal University
Irina Svistunova
Far Eastern Federal University
Galina Tretyakova
Far Eastern Federal University
Zahar N. Puzyr'kov
Far Eastern Federal University
Vitaliy Vovna
Far Eastern Federal University

Research Article

Keywords: electronic structure, photoelectron spectroscopy, density functional theory, outer-valence Green's function (OVGF) method, ADC(2), spiroborate complexes

Posted Date: October 26th, 2022

DOI: https://doi.org/10.21203/rs.3.rs-2174168/v1

License: This work is licensed under a Creative Commons Attribution 4.0 International License.
Read Full License

Abstract

Electronic structure, cationic and excited states of three spiroborate complexes (2-acetylacetonato-1,3,2-benzodioxaborol, its NH- and NMe-derivatives) and three corresponding ligands (acetylacetone, 4-aminopent-3-en-2-one and 4-methylaminopent-3-en-2-one) were studied by photoelectron spectroscopy, absorption spectroscopy, high-level ab initio quantum chemical computations, including the algebraic diagrammatic construction method for the polarization propagator of the second order, the outer-valence Green's function method, the density functional approach, and the time-dependent density functional approach. Analysis of experimental and calculated data allowed determining the influence of functional groups on the parameters of the electronic structure and energy of electronic transitions. Compared to acetylacetone and its NH- and NMe-derivatives, the upper filled molecular orbitals of the corresponding spiroborates are stabilized at 0.4–1.7 eV, which is due to the positive charge of the ligand due to the acceptor properties of the dioxyphenylene fragment. Among the studied compounds, when replacing the oxygen atom in the α-position with the NH- or NMe-group, a bathochromic shift of intense bands in the absorption spectra is observed, since the energy intervals between the orbitals of the π_3 and π_4 ligand are reduced. In addition, in a number of spiroborates, the violation of C_{2v} symmetry when replacing an oxygen atom leads to the appearance of a low-intensity maximum in the long-wave part of the absorption spectrum, due to the $\pi_2^X \rightarrow \pi_4$ transition.

1. Introduction

Boron difluoride β-ketoiminates are structural and electronic analogs of boron difluoride β-diketonates, which have not been sufficiently studied to date. This class of compounds has weak luminescence in diluted solutions [1–3], but intensively luminesces in the crystalline state and is a promising class of luminophores [3–6].

Among such boron complexes, unconjugated phosphor complexes such as spiroborates are of particular importance. They often show intense fluorescence in the solid state and weak fluorescence in the solution, which determines their use as markers of metal ions [7]. Due to their thermal and chemical stability, they are the basis of ionic organic sensors that detect H_2 and CH_4 gases [8]. Materials based on spiroborates are also used in medicine, for example, as a carrier for the drug, increasing its bioavailability and absorption by the human body [9, 10]. Some complexes are effective catalysts in reducing reactions, in particular, in the reduction of aryl alkyl and halogenated ketones [11], as well as in the synthesis of pyranonaphthoquinone antibiotics [12]. In industry, spiroborate anions coupled with tetraalkylphosphonium, pyrrolidinium, and imidazolium cations are used in ionic liquids [13–15]. These compounds can be used as alternative high-performance lubricants [16, 17].

Determining the dependence of consumer properties on the electronic structure opens up opportunities for directional synthesis of spiroborates. The most reliable information about the electronic structure can be obtained by the joint application of photoelectron spectroscopy and quantum chemistry. The use of the absorption spectroscopy method and the results of modeling excited states allows assessing the

effect of substituents on spectral characteristics [18–19]. With a good agreement between the theory and the experiment, it is possible to judge the quality of the results of quantum-chemical modeling.

The methods of Green's functions [20] allow determining the nature of overlapping bands in the photoelectronic spectra of small molecules. Among them, one can distinguish the highly specialized outer-valence Green's function (OVGF) method [21]. This approach uses the third-order approximation of perturbation theory and is used to calculate transition energies into cationic states, which are well described in terms of single-electron ionization for upper valence orbitals. However, when simulating the cationic states of chelated complexes, the calculation time of the OVGF method increases proportionally to n^5 relative to the number of molecular orbitals. Therefore, when interpreting photoelectronic spectra of coordination compounds of boron, the density functional theory (DFT) analog of the Koopmans theorem is often used [22, 23].

At the same time, time-dependent density functional theory (TDDFT) approximation [24, 25] is widely used in modeling excited states of boron chelated complexes. However, as shown in [26, 27], the TDDFT method can be successfully applied only for single excited states, which significantly limits the use of this method. Therefore, where possible, non-empirical computational methods should be used, such as: configuration interaction [28], multi-configuration self-consistent field [29], related clusters [30], as well as methods of algebraic diagrammatic construction (ADC) [31] in the second and third order of perturbation theory (ADC(2) and ADC(3)). Among them, ADC methods should be noted, the advantages of which are: dimensional coherence, comparative economy, as well as direct calculation of energies and moments of transition, which avoids errors associated with the unbalanced description of the initial and final states [32, 33]. When calculating the excited states of boron chelate complexes [34], the domain-based local pair natural orbital (EOM-DLPNO) method is also used [35, 36], which is a highly specialized approach for studying large molecular systems at significantly lower computational costs.

This paper presents the results of the study of the electronic structure and cationic and excited states of three spiroborates and three corresponding ligands (Scheme 1) according to the methods of photoelectron spectroscopy, absorption spectroscopy and simulation results. The OVGF and DFT methods were used in the calculation of cationic states, and ADC(2), TDDFT and EOM-DLPNO methods were used in the modeling of excited states.

2. Experimental And Theoretical Methods

2-Acetylacetonato-1,3,2-benzodioxoborol (IV) was synthesized from benzoylacetone according to the reported method [37]. 4-aminopent-3-en-2-one and 4-methylaminopent-3-en-2one were obtained according to the procedures described earlier [38, 39]. 2-(4-methylaminopent-3-en-2-one)-1,3,2-benzodioxoborol (VI) was synthesized according to the reported method [40]. Solvents were obtained from EKOS-1 and used without additional purification.

Synthesis of 2-(4-aminopent-3-en-2-one)-1,3,2-benzodioxoborol (V):

A solution of 0.00798 mol of 4-aminopent-3-en-2-one was boiled with a Dean-Stark trap, with an equimolar amount of dioxophenylenebutylborate (pyrocatechinylbutoxyborate, ρ = 1.072 g/ml) in 50 ml of toluene, for 4–6 hours. The resulting solution was cooled to room temperature and left overnight in the refrigerator for crystallization. The resulting white precipitate was filtered off, the reaction yield was 80%, recrystallized from ethanol. m.p. 300°C.. IR (KBr): 3144, 3192, 3204 (νN-H), 3029 (C-H), 1531, 1595 (C = C, C = O), 1366 (νB-O). MS: m/z calculated for $C_{11}O_3NBH_{11}$: 216; found: 217 [M + 1]. IR spectra (KBr disks, oil) were recorded on Shimadzu IR Prestige-21. Mass spectra were recorded in the positive and negative ion modes (electrospray ionization ESI, a Shimadzu LCMS 2010EV mass spectrometry detector); the samples were injected into the acetonitrile-water system (9:1). UV-visible absorption spectra were recorded using a spectrophotometer 2550 (Shimadzu-UV) with a quartz cuvette (path length 1 cm).

X-ray photoelectronic spectra of compounds IV and VI in the condensed state were measured using a two-chamber high-vacuum system MXPS XP (manufactured by Omicron, Germany) with a hemispherical electrostatic analyzer (radius 125 mm). The radiation energy was 1253.6 eV (Mg Kα). The scattering function of the spectrometer in the mode of recording characteristic atomic levels had a half-width of 1.2 eV. Electron binding energy (E_b) calibration was performed on the 1s carbon level. When assessing the atomic concentration of elements in the sample, the relative ionization cross-sections and the electron yield depth were taken into account. The relative concentration of elements obtained from the intensities of the bands corresponding to 1s-electrons coincided with the one calculated within the error of the method (10%).

Previously [41–46], it was shown that the geometry of boron chelated complexes in the S_0 state could be successfully optimized in the approximation of DFT with a set of atomic functions Def2-SVP and the B3LYP function [47]. Therefore, the geometry of compounds I–VI was optimized by the DFT/B3LYP/Def2-SVP method. To verify the compliance of the optimized structures with the points of the local minimum on the surface of the potential energy, the Hesse matrix was calculated for all connections [48].

When interpreting photoelectronic spectra, the results of calculations by the OVGF/cc-pVDZ method were used as a reference [49, 50], which allows obtaining absolute energies of cationic states with an average error of 0.2–0.3 eV. In addition, to compare the experimental values of ionization energies with the energies of the Kohn – Sham (KS) ε_n orbitals, the DFT analog of the Koopmans theorem was used [22, 23]:

$I_n = -\varepsilon_n + \delta$,

where I_n is ionization energy; F;

ε_n is the single-electron energy KS;

δ is the value of the correction to the orbital energy.

In [51], it was shown that the use of DFT calculations allowed obtaining qualitative results when calculating the cationic states of boron chelated complexes. A good correlation with experimental data is explained by the similarity of KS equations with quasiparticle Dyson's equations [22].

However, the DFT method does not always provide reliable information about the sequence of electronic levels [22]. At the same time, the use of DFT calculations with the CAMB3LYP functionality gives a good correlation with the intervals of the energies of cationic states according to the OVGF method [51]. Therefore, the energy of electron levels in the S_0 state and the distribution of electron density at each MO were obtained by the DFT/CAMB3LYP/cc-pVDZ method [52].

The results of TDDFT, ADC(2), and DLPNO calculations were used in the interpretation of absorption spectra. The energies of excited states were obtained by the TDDFT/CAMB3LYP/cc-pVDZ method [53]. To clarify the energies and forces of oscillators of excited states, the ADC method was used (2). Also, the EOM-DLPNO method was used to estimate the energies of the maximums of the bands in the optical spectra. All calculations of excited states were carried out in a correlation-consistent polarized basic set of atomic functions cc-pVDZ [54].

All DFT and TDDFT calculations were carried out in the GAMESS software computing package (US). ADC(2) calculations of excited states were performed using the Orca software package [55]. DLPNO calculations were carried out in the Gaussian software package [56].

3. Results And Discussion

3.1. Electronic Structure

Table 1 shows the experimental and calculated ionization energy (I_n) values for compounds I–III, as well as the contributions of the orbits of the oxygen atom O, the carbonyl carbon atoms of the C_β, the CH group at the γ-position, the methyl groups and the OH groups (compound I), NH_2 (compound II), NHMe (compound III), denoted as X. For the filled orbits, the contributions of the Mulliken atomic populations are given, and for the vacant MO, the relative sums of the squares of the coefficients of the base orbits. Orbitals are mixed if the sum of the Mulliken atomic populations for each of the fragments is greater than 20%. The “+” sign indicates binding and the “–” sign indicates anti-binding.

In the row of compounds I–III, a correlation of the nature of the three upper filled MOs is observed. According to the OVGF/cc-pVTZ method, the substitution of the OH group with the NH_2 group leads to a decrease in I_{1-3} by 0.72–1.12 eV and destabilization of the energy of affinity for the electron by 0.41 eV (Table 1). The substitution of the amino group for the NMe group determines a reduction of I_{1-3} by 0.15–0.51 eV, but has no appreciable effect on the energy of the electron affinity. Therefore, the substitution of the OH group with the NH_2 and NMe groups causes a decrease in the HOMO→Lumo energy gap value by 0.54 and 0.94 eV, respectively, which leads to a bathochromic shift in the absorption spectra (Fig. S1).

The transition from ligands (Compound I–III) to spiroborates (Compound IV–VI) stabilizes the energy of affinity for the electron by 1.4–2.0 eV (Fig. 2, Table 1). At the same time, π_3 MOs are stabilized by 0.8–1.0 eV, which leads to a decrease in the energy interval $\pi_3 \rightarrow \pi_4$ by 0.7–1.1 eV. For the remaining upper filled ligand orbits, there is also stabilization of levels at 0.4–1.7 eV. This is due to the transfer of electron density 1.04–1.08 *e* from the ligand to dihydroxyphinylene.

Fig. 1 shows the MO forms needed for further discussion. Table 1 presents experimental and calculated I_n values for compounds IV–VI, types of valence MOs KS, as well as contributions of atomic orbits localized on fragments of the molecule (ligand – $O(X)C_3H$, dihydroxyphenylene – PhO_2B, substitute – 2Me). The types of the Kohn-Sham molecular orbitals are determined relative to the Mulliken atomic populations. Type π orbitals are divided into localized on the ligand and on dihydroxyphenylene (indicated by the supreme index X). The correlation diagram of *In* (OVGF/cc–pVTZ) in Fig. 2 is provided to demonstrate the electronic effects of substitution.

Table 1 Relative vertical ionization energies (eV) of the highest occupied MOs (denoted as H,..., H–n) and electron affinities of the lowest unoccupied MO (denotes as L) in IV-VI computed using the Hartree-Fock approach at the level of the Koopmans' theorem (HF), the OVGF and DFT/CAMB3LYP methods (cc-pVDZ basis set). The Mulliken populations of the molecular fragments in the molecular orbitals (percent) are also shown.

MO, type	Contribution, %			Ionization energies, eV		
	$PhO_2B/2O$	$O(X)C_3H/OX$	2Me	HF	OVGF	CAMB3LYP
Compound IV						
L, a_2 π_4	1/0	83/13	16	−1.61	0.18	1.00
H, b_2 π_2^X	99/14	1/0	0	7.47	7.12	6.51
H−1, a_2 π_3^X	100/6	0/0	0	8.42	8.06	7.43
H−2, b_1 π_3	3/2	94/21	3	10.43	9.66	9.00
H−3, b_2 π_1^X	94/19	5/4	1	12.17	10.71	10.12
H−4, a_1 σ^X	100/19	0/0	0	12.64	11.05	10.60
H−5, b_2 n_-	10/0	73/48	17	13.21	11.47	10.61
H−7, b_1 σ^X	95/25	3/1	1	13.43	11.81	10.74
H−6, a_2	84/70	13/10	3	13.64	11.73	11.14
H−8, b_1	100/66	0/0	0	13.89	12.04	11.93
H−9, a_1 σ^X	98/24	2/1	0	14.78	12.90	12.36
H−11, a_2 π_2	18/14	46/41	36	15.20	13.57	12.49
H−10, a_1 n_+	19/4	62/37	19	15.23	13.45	12.73
H−12, b_1 π_1	19/5	38/28	43	15.31	13.80	12.96
Compound V						
L, π_4	1/0	87/19	12	−2.23	0.41	0.40
H, π_2^X	99/15	1/1	0	7.36	6.99	6.37
H−1, π_3^X	100/6	0/0	0	8.36	7.97	7.34
H−2, π_3	3/2	94/27	2	9.63	8.90	8.32
H−3, π_1^X	91/20	8/6	2	12.02	10.55	9.94
H−4, σ^X	100/20	0/0	0	12.53	10.92	10.01
	60/39	34/22	6	13.10	11.48	10.33

H−5, $\sigma^{x} + \pi_2$						
H−6, n_-	17/0	68/43	16	13.23	11.54	10.56
H−7, σ^{x}	81/39	15/12	3	13.33	11.62	10.71
H−8, σ^{x}	99/53	1/1	0	13.74	11.93	11.05
H−9, σ^{x}	49/37	39/27	12	14.25	12.58	11.78
H−10, σ^{x}	97/23	2/1	1	14.67	12.78	11.83
H−11, Me + π_1	20/10	36/30	44	14.95	13.39	12.34
H−12, $n_+ + \sigma^{x}$	50/18	24/15	26	15.19	13.48	12.56
Compound VI						
L, π_4	1/0	84/17	15	−2.17	0.38	0.38
H, π_2^{x}	99/15	1/1	0	7.38	6.99	6.39
H−1, π_3^{x}	100/6	0/0	0	8.39	7.99	7.37
H−2, π_3	3/2	94/28	2	9.37	8.60	8.07
H−3, π_1^{x}	88/20	10/7	2	12.02	10.54	9.93
H−4, σ^{x}	100/20	0/0	0	12.54	10.91	10.02
H−5, π_2	19/14	74/35	7	12.77	11.40	10.33
H−6, $n_- + \pi_1^{x}$	20/1	66/37	14	13.00	11.35	10.53
H−7, σ^{x}	90/41	8/5	2	13.29	11.56	10.57
H−8, σ^{x}	95/56	4/1	1	13.73	11.90	11.07
H−9, σ^{x}	80/54	17/4	3	13.85	12.05	11.26
H−10 σ^{x}	91/22	7/2	2	14.67	12.79	11.84
H−11, $n_+ + \sigma^{x}$	27/9	65/10	8	14.88	13.39	12.26
H−12, Me + π_1	21/12	35/30	44	14.92	13.32	12.38

Table 2 Relative vertical ionization energies (eV) of the highest occupied MOs (denoted as H,..., H−n) and electron affinities of the lowest unoccupied MO (denotes as L) in I-III computed using the Hartree-Fock approach at the level of the Koopmans' theorem (HF), the OVGF and DFT/CAMB3LYP methods (cc-pVDZ

basis set). The Mulliken populations of the molecular fragments in the molecular orbitals (percent) are also shown.

MO, type	Contribution. %					Ionization energies. eV			
	O	$2C_{\beta}$	$C_{\gamma}H$	2Me	X	HF	OVGF	CAMB3LYP	Expt data
Compound I									
L, π4	15	49	3	25	8	−2.80	−1.22	0.04	-
H, π3	13	15	51	4	17	9.49	8.90	8.26	9.08
H−1, n-	60	9	9	13	9	11.39	9.76	8.88	9.69
H−2, π_2	37	16	1	25	21	13.71	12.50	11.50	12.5
H−3, n_+	11	12	25	8	43	14.63	13.02	11.87	
H−4, Me−π_1	8	10	3	51	29	14.83	13.41	12.29	13.2
H−5, Me−σ	10	11	9	67	3	14.90	13.61	12.40	
H−6, Me	2	4	1	88	5	15.54	14.46	13.10	14.2
H−7, σ+Me	15	21	11	42	11	16.07	14.56	13.44	
H−8, σ	8	15	1	73	4	16.47	14.63	13.56	
H−9, Me+π_2	15	25	5	37	17	16.26	15.13	13.87	
H−10, π_1+Me	6	26	7	45	16	17.04	15.52	14.48	
Compound II									
L, π_4	15	55	6	14	10	−3.17	−1.63	−0.43	–
H, π_3	13	11	48	2	25	8.54	7.95	7.43	8.24
H−1, n_-	66	8	9	13	3	10.70	9.04	8.17	8.98
H−2, π_2	32	21	0	18	30	12.59	11.38	10.58	11.2
H−3, π_1−Me	14	18	8	39	21	13.65	12.38	11.51	12.0
Compound III									
L, π_4	14	55	5	13	13	−3.18	−1.59	−0.47	
H, π_3	13	9	47	2	29	8.26	7.59	7.15	7.81
H−1, n_-	66	8	8	13	5	10.58	8.89	8.07	8.74
H−2, π_2	26	23	2	12	37	12.08	10.87	10.20	10.6
H−3, π_1−Me	21	20	9	36	15	13.35	12.11	11.27	11.6

According to the calculated data of the DFT method, in compound IV, the π-orbitals of acetylacetone and dihydroxyphenylene are not mixed up to 13.5 eV, where the mixing is negligible. A similar pattern is observed due to the mutually perpendicular arrangement of the planes of acetylacetone and dihydroxyphenylene. Thus, the types of MOs of Compound IV can be divided into two groups: localized on acetylacetone and on dihydroxyphenylene. The OVGF/cc–pVTZ method showed that the highest occupied molecular orbital (HOMO) (I_1 = 7.12 eV), HOMO-1 (I_2 = 8.06 eV), and HOMO-3 (I_4 = 10.71 eV) corresponded to π^X -orbitals, and HOMO-4, HOMO-6, and HOMO–9 are σ^X-orbitals of dihydroxyphenylene. There are also two MOs at 11.73 eV and 12.04 eV localized mainly on oxygen atoms of dihydroxyphenylene. The three filled π-orbitals of acetylacetone correlate with I_3, I_{11} and I_{13} at 9.66, 13.57 and 13.8 eV, respectively. The n_- and n_+ orbitals, located predominantly on oxygen atoms, were determined by the OVGF/cc–pVTZ method as I_6 = 11.47 eV and I_{12} = 13.45 eV, respectively. The lowest unoccupied molecular orbital (LUMO) is defined as the π-orbital of acetylacetone, and the energy of electron affinity is 0.18 eV.

The replacement of an oxygen atom with an NH group (compound V) leads to the stabilization of the LUMO level by 0.23 eV and the destabilization of the HOMO level by 0.13 eV (Table 1, Fig. 2). These orbitals are localized on fragments located relative to each other at an angle close to 90°, so a decrease in the energy gap by 0.36 eV should not affect the optical spectra of the connections, since in the considered complexes, the transition $\pi_2^X \rightarrow \pi_4$ is prohibited by the selection rules for symmetry C_{2v}. While destabilization of the π_3 level by 0.76 eV leads to a decrease in the $\pi_3 - \pi_4$ interval, which causes a bathochromic shift of the long-wave band in the absorption spectrum. Replacing the NH- group with NMe- (compound VI) destabilizes the π_3 level by 0.30 eV. At the same time, in all spiroborates, MOs localized on the dioxyphenylene fragment change their energy within the range of 0.01–0.03 eV (Table 1, Fig. 2), and the change in the energies of the electron levels of the ligands is associated with the replacement of the oxygen atom in the structure of the ligand of the NH- and NMe-group. The addition of the dioxyphenylene moiety stabilizes the n_- orbital by mixing (in the order of 10–18%) with π_1^X. Mixing π_2^X MO with oxygen AO (15%) destabilizes the orbital, resulting in the inversion of π_2^X and π_3^X MOs.

According to the calculated data, energy splitting of C 1s-electron levels is observed in the studied complexes (Fig. S2). Depending on the energy, the levels of C 1s-electrons can be divided into three groups C 1s, C 1s' and C 1s" (Fig. S2). The first group includes the levels of carbon atoms in the meta and para positions of the benzene cycle (colored green and red, respectively). Group C1s' includes the levels of methyl group carbon atoms and the benzene cycle in the ortho- position. The electron levels of carbonyl carbon atoms are colored yellow and designated as C 1s". The deviation from C_{2v} symmetry when replacing an oxygen atom with NH- and NMe-groups, as well as the transfer of the charge from the substituent to the carbon atom at the β-position and methyl groups (about 35%) leads to the cleavage of degenerate levels of C1s' and C1s".

According to the calculated data, the point group of symmetry of the molecule of boron acetylacetonate of 1,2-dihydroxyphenylene (compound – IV) is close to C_{2v}. The deviation of the plane of acetylacetone

from the plane perpendicular to the dihydroxyphenylene group is 8.2°. When replacing an oxygen atom in the α-position with NH- and NMe-groups (compounds V and VI), the deviation of the plane of acetylacetone from the plane perpendicular to the dihydroxyphenylene group is 0.8° and 0.4°, respectively. The interatomic distances B-O1 and B-O2 (1.43 Å) are less than B-O3 and B-O4 (1.51 Å), and when O4 is replaced with an NH group, the distances B-O1 and B-O2 increase to 1.45 Å, with B –N = 1.55 Å and B-O3 = 1.5 Å.

3.2. Photoelectronic spectra

Earlier, the authors of this paper published a thorough analysis of X-ray photoelectron spectroscopy (XPS) data for Complex IV [57]. In this paper, the results of calculations of complexes I–III, IV, VI are compared with ultraviolet photoelectron spectroscopy and XPS spectra to obtain comprehensive information about electronic levels and identify substitution effects.

In accordance with the simulation results using the methods DFT/CAMB3LYP/cc-pVTZ (Koopmans extended theorem) and OVGF/cc-pVTZ, the bands “1” and “2” in compound I are determined by single-electron ionization processes (Fig. 3). Arm “3 ‴ corresponds to two electronic levels. The bands “3”, “4” and “5” are due to two, five and two cationic states, respectively.

In compounds II and III, bands “1” and “2” are determined by single-electron ionization processes, and there is an increase in energy intervals between I_3 and I_4 (Fig. 3, Table 1), compared to I. Therefore, the band “3” in II and III corresponds to one electronic level. In Compounds II and III, arm “4 ‴ is caused by ionization from a single orbital, and band 4 is related to two and three cationic states, respectively.

In the XPS spectra of the valence region of compounds IV and VI, two intensity maximums are observed in the energy range from 1.0 to 13.0 eV, two maximums in the energy range from 13.0 to 22.0 eV, and one maximum at 28.0 eV (Fig. 4). The relative intensities and contours of the components are determined by the distribution of the density of electronic states and the relative ionization cross-sections of 2s- and 2p-levels (σ_s, σ_p). For the source Mg Kα, the ratio σ_s:σ_p for carbon is 17.9, for oxygen 5.8 and for nitrogen 10.6, and the ratio σ_p (C):σ_p(N):σ_p(O) is 1.0 : 3.2 : 8.9 [58].

The results of quantum chemical modeling by the methods of DFT/CAMB3LYP/cc-pVTZ and OVGF/cc-pVTZ showed that the maximums “1” and “2” in the spectra of both compounds, as well as the inflections “1‴ and “1⁗” in the spectra, are due to the predominant ionization with O 2p AOs. The “3” maxima correspond to mixed C 2s / O 2p AOs. The “4” maxima are determined by ionization from C 2s orbitals. The “5” maximum in compound IV is determined by ionization with four MOs with predominant contributions of O 2s AOs. In compound VI, two maxima are observed in the last band of the spectrum. At the same time, the contribution to the “5” maximum is given by O 2s and N 2s AOs.

On the X-ray spectra of C 1s-electrons of complexes IV and VI (Fig. S3), two components C 1s and C^{β} 1s are present. The calculated energy values that determine the half-width and the position of the maximums of the bands in the scale of communication energies are presented on the XPS spectra of C

1s-electrons of compounds IV and VI (Fig. S3). For C1s electrons in compounds, the low-energy group of levels is due to ionization from the carbon atoms of the benzene cycle. The levels of the two carbonyl carbon atoms are shifted by 3.5–4.5 eV, and the central group of levels corresponds to the remaining carbon atoms. The overlapping bands of the two groups of levels in the range of E_b 284.0–286.5 eV cause a half-width of 2.3–2.5 eV for the entire band with a maximum at 285.5 eV. On the XPS spectra of C 1s levels, a good correspondence is observed between the differences in energy and the relative areas of the Gaussians with the calculated energies and the number of electronic levels (Fig. S3).

For both complexes, as for most boron chelate complexes [59, 60], the binding energy of 1s-electrons of the boron atom is 193.1 eV (Table S1), which, according to the table data [61], is characteristic of a high degree of oxidation of the boron atom. The concentration values obtained experimentally showed a good agreement with the concentrations according to the gross formula. The deviation did not exceed 2.2 % for carbon and oxygen and 0.7 % for boron and nitrogen.

3.3. Excited states

To interpret the absorption spectra of compounds IV–VI (Fig. 5), Table 3 presents the calculated characteristics of significant transitions in comparison with the experimental data of the absorption spectroscopy method. To assess the effect of the dioxyphenylene moiety on the spectral-luminescent characteristics of compounds IV–VI (Fig. 5), Table 3 presents the results of calculations of excited states of ligands I–III.

In the spectra of compounds IV–VI, the intense band corresponds to the excited state S_2 (Fig. 5, Table 3). This state with an oscillator force of 0.205 is determined by the transition $\pi_3 \rightarrow \pi_4$. The excited states S_1, S_3, and S_4 (S_5 for compound IV) are prohibited by the selection rules and have a low oscillator strength according to the simulation results. Despite this, the spectra of compounds V and VI show a low-intensity maximum in the long-wave part of the spectrum. Since the selection rules are strict for ideal C_{2v} symmetry, this phenomenon for compounds V and VI is explained by a deviation from C_{2v} symmetry by replacing one oxygen atom with an NH- or NMe-group. In the short-wave part of the theoretical spectrum, a band defined by the excited state of the phenylene (transition $\pi_3^X \rightarrow \pi_4^X$) should also be observed.

Table 3. Excited states in IV–VI calculated and experimental. The oscillator strength is indicated in brackets.

Compd	State (№)	Transition	hv, eV			
			ADC(2)	EOM-DLPNO	TDDFT/ CAMB3LYP	Expl data
IV	1	$\pi_2^{x} \rightarrow \pi_4$	3.41 (0.0020)	3.91 (0.0035)	3.38 (0.0039)	3.56
	2	$\pi_3 \rightarrow \pi_4$	4.48 (0.2054)	4.33 (0.2892)	4.58 (0.0315)	4.40
	3	$\pi_3^{x} \rightarrow \pi_4$	4.71 (0.0197)	4.68 (0.0400)	4.97 (0.2456)	
	4	$n_{-} \rightarrow \pi_4$	5.04 (0.0026)	5.07 0.0014	5.21 (0.1010)	
	5	$\pi_2^{x} \rightarrow \pi_4^{x}$	5.10 (0.0902)	5.39 (0.0751)	5.30 (0.0212)	
V	1	$\pi_2^{x} \rightarrow \pi_4$	3.81 (0.0001)	4.25 (0.0012)	3.78 (0.0002)	3.55
	2	$\pi_3 \rightarrow \pi_4$	4.49 (0,1911)	4.27 (0.2646)	4.87 (0.2191)	4.33
	3	$\pi_2^{x} \rightarrow \pi_4^{x}$	5.00 (0,0294)	4.66 (0.0511)	5.02 (0.0040)	
	4	$\pi_3^{x} \rightarrow \pi_4$	5.25 (0,1186)	5.82 (0.1419)	5.21 (0.1667)	
	5	$n_{-} \rightarrow \pi_4$	5.90 (0,0000)	5.91 (0.0009)	5.87 (0.0230)	
VI	1		3.77	4.14	3.83	3.51

	$\pi_2^{X} \rightarrow \pi_4$	(0.0001)	(0.3026) $\pi_3 \rightarrow \pi_4$	(0.0002)	
2	$\pi_3 \rightarrow \pi_4$	4.34 (0.2303)	4.25 (0.0019) $\pi_2^{X} \rightarrow \pi_4$	4.71 (0.2678)	4.11
3	$\pi_2^{X} \rightarrow \pi_4^{X}$	4.98 (0.0294)	4.25 (0.0016) $\pi_2^{X} \rightarrow \pi_4$	5.05 (0.0022)	
4	$\pi_3^{X} \rightarrow \pi_4$	5.22 (0.1195	5.25 (0.0560)	5.22 (0.1697)	
5	$n_{-} \rightarrow \pi_4$	5.85 (0.0002)	5.83 (0.0192) $\pi_3^{X} \rightarrow \pi_4$	5.85 (0.0217)	

The replacement of the oxygen atom with an NH group (complex V) leads to a bathochromic shift of 0.07 eV, and the replacement of the NH group with NMe increases the shift to 0.29 eV, which is consistent with the calculated data on the change in the energy interval between MO π_3 and π_4.

Table 4 presents the results of simulating the excited states of compounds I–III according to the ADC(2)/cc–pVTZ, DLPNO/cc–pVTZ, and TDDFT/CAMB3LYP/cc-pVTZ methods. In absorption spectra I–III, the long-wave bands correspond to the excited state with a transition of $\pi_3 \rightarrow \pi_4$. According to the calculations and experiment data, there is a decrease in the energies of the excited states S_1 and S_2 during the transition from I to II and III, which correlates with the data on changes in the value of the HOMO→LUMO energy gap.

Table 4 Excited states in I–III calculated and experimental. The oscillator strength is indicated in brackets.

Compd.	State (№)	Transition	hv, eV			
			ADC(2)	EOM-DLPNO	TDDFT/ CAMB3LYP	Expl data
I	1	$n_- \rightarrow \pi_4$	4.17 (0.0004)	4.22 (0.0006)	4.45 (0.0005)	4.53
	2	$\pi_3 \rightarrow \pi_4$	5.06 (0.2646)	4.85 (0.3601)	5.23 (0.3023)	
II	1	$n_- \rightarrow \pi_4$	4.02 (0.0002)	4.08 (0.0005)	4.31 (0.0003)	4.22
	2	$\pi_3 \rightarrow \pi_4$	4.79 (0.3037)	4.46 (0.3629)	4.98 (0.3301)	
III	1	$n_- \rightarrow \pi_4$	3.97 (0.0002)	4.09 (0.0004)	4.31 (0.0004)	3.99
	2	$\pi_3 \rightarrow \pi_4$	4.49 (0.3398)	4.18 (0.3939)	4.77 (0.3814)	

For all compounds, a qualitative correspondence between the experimental and calculated absorption spectra is observed (Fig. 5). The DLPNO method, in comparison with the ADC(2) and TDDFT methods, allowed a better agreement with the experiment for the oscillator forces and the absolute values of the energies of the excited states (Table 5). Despite this, this method overestimates the energy of the forbidden transition in the range of 3.4–3.6 eV by an average of 0.5 eV, which leads to difficulties in interpreting the absorption spectra. Due to the well-chosen parameters of the CAMB3LYP function, the TDDFT calculation data on the oscillator forces are better consistent with the experiment compared to the ADC(2). However, the TDDFT method significantly inflates the transition energy $\pi_3 \rightarrow \pi_4$, so the interpretation of the spectra was carried out according to the ADC method (2).

Table 5 Deviations of the calculated data for the energies of excited states from the experimental data for compounds I–VI

Method	Error, eV					
	I	II	III	IV	V	VI
TDDFT/CAMB3LYP	0.71	0.76	0.79	0.60	0.65	0.60
ADC(2)	0.54	0.57	0.51	0.08	0.19	0.22
EOM-DLPNO	0.33	0.25	0.21	0.08	0.05	0.00

Conclusion

For 2-acetylacetonato-1,3,2-benzodioxaborol, its NH- and NMe-derivatives, and three corresponding ligands (acetylacetone, 4-aminopent-3-en-2-one and 4-methylaminopent-3-en-2-one), the data analysis of the photoelectron spectroscopy, absorption spectroscopy, OVGF/cc-PVDZ, DFT/CAMB3LYP/cc-PVDZ, ADC(2)/cc-PVDZ and EOM-DLPNO/cc-PVDZ methods was carried out. Evaluation of the effect of substituents on the localization of electron density, the energy of cationic states, electron affinity, and excited states was carried out on the basis of modeling results by the most reliable methods for such systems OVGF/cc-PVDZ and ADC(2)/cc-PVDZ.

Among the studied spiroborates and corresponding ligands, the replacement of the oxygen atom in the α-position by the NH- or NMe- group leads to a decrease in the energy intervals between π_3 and π_4 MOs by 0.54–1.26 eV, which determines the bathochromic shift of the intense band in the absorption spectra by 0.07–0.29 eV.

It was found that dihydroxyphenylene at the boron atom (in spiroborates) due to its acceptor properties (– 1.04–1.08 *e*) stabilized the upper filled MOs of ligands by 0.4–1.7 eV.

In the absorption spectra of spiroborates, the intense maximum corresponds to the excited state S_2 with the $\pi_3 \rightarrow \pi_4$ transition. The excited state S_1 ($\pi_2^X \rightarrow \pi_4$ transition) of 2-acetylacetonato-1,3,2-benzodioxaborolis prohibited by the selection rules for C_{2V} symmetry and therefore a low-intensity band in the long-wave part of the absorption spectrum is observed only for its NH- and NMe-derivatives.

The obtained data can be used for the development of new optical functional materials based on boron compounds, which are promising for devices for converting and processing optical signals, optical sensors, and optoelectronics.

Declarations

ACKNOWLEDGEMENTS

The research was carried out with the financial support of the Russian Foundation for Basic Research (grant No. 20–33–90196 “Graduate Students”). S.A.T. is grateful to the Ministry of Science and Higher Education of the Russian Federation (Grant No. 075-01471-22). The software packages GAUSSIAN 16 and Orca 4.2.1 helped to make calculations using the computing resources of the “Computer Center of St. Petersburg University” Resource Center (http://cc.spbu.ru). Test calculations were performed at the equipment of Shared Resource Center “Far Eastern Computing Resource” IACP FEB RAS (https://cc.dvo.ru).

Ethical Approval:

Not applicable.

Competing interests:

All authors have read and approve this version of the article, and due care has been taken to ensure the integrity of the work. No conflict of interest exists in the submission of this manuscript.

Authors' contributions:

Andrey Sidorin: Methodology, Writing - original draft, Writing - review & editing, Validation, Visualization, Analysis.
Sergey Tikhonov: Conceptualization, Resources, Investigation, Analysis, Validation, Supervision.
Ilya Samoilov: Resources, Investigation.
Ivan Osmushko: Resources, Investigation.
Irina Svistunova: Resources, Investigation.
Galina Tretyakova: Resources, Investigation.
Zahar Puzyrkov: Resources, Investigation.
Vitaliy Vovna: Supervision, Funding acquisition.

Funding:

The research was carried out with the financial support of the Russian Foundation for Basic Research (grant No. 20–33–90196 “Graduate Students”). Tikhonov S.A. is grateful to the Ministry of Science and Higher Education of the Russian Federation (Grant No. 075-01471-22).

References

1. V.E. Karasev, A.G. Mirochnik, E.V. Fedorenko, *Photophysics and Photochemistry of β-Diketonates of Boron Difluoride, Dal’nauka*, Vladivostok, 2006 [in Russian].
2. V.E. Karasev, O.A. Korotkih, *Spectral-luminescent properties of fluoride-boron difluoride β-diketonates*, J. Inorg. Chem., 1986 [in Russian].
3. A.P. Skoldinov, V. G. Medvedeva, *Method for obtaining BF2O-complexes of β-dicarbonyl compounds* № 846375/23–4, 1964 [in Russian].
4. C.R. Hauser, F.W. Swamer, and J.T. Adams, "Organic Reactions," Vol. VIII, ed. by R. Adams, A.H. Blatt, V. Boeckelheide, A.C. Cope, D.Y. Curtin, F.C. McGrew, and C. Niemann, John Wiley & Sons, Inc., New York, 1954, pp. 59–196.
5. H. C. Walker, J.J. Sanderson, C.R. Hauser, Acetoacetylation of aromatic compounds by boron fluoride to form β-diketones. Failure with boron and aluminium chloride, J. Am. Chem. Soc. 75 (1953) 4109–4110. https://doi.org/10.1021/ja01112a534.
6. B. Stefane, S. Polanc, New and a convenient route to enaminones and pyrazoles, New J. Chem. 26 (2002) 28–32. https://doi.org/10.1039/b108524g.
7. H.S. Kumbhar, S.S. Deshpande, G.S. Shankarling, Novel, solid-state, highly fluorescent β-ketoiminate spiroborates with aggregation induced emission, Dyes Pigm. 127 (2016) 161–169.

https://doi.org/10.1016/j.dyepig.2016.01.006.

8. Y. Du, H. Yang, J.M. Whiteley, S. Wan, Y. Jin, S.-H. Lee, W. Zhang, Ionic covalent organic frameworks with spiroborate linkage, Angew. Chem. Int. Ed. Engl. 55 (2016) 1737–1741. https://doi.org/10.1002/anie.201509014.
9. J. John, S. Rugmini & B.S. Nair, Effect of the substituent on the thermal stability of spiroborate esters of curcumin, J. Therm. Anal. Calorim. 139 (2020) 3537–3547. https://doi.org/10.1007/s10973-019-08739-y.
10. S. Anjana, J. Joseph, J. John, S. Balachandran, T.R.S Kumar, A. Abraham, Novel flourescent spiroborate esters: potential therapeutic agents in in vitro cancer models, Mol. Biol. Rep. 45 (2019) 727–740. https://doi.org/10.1007/s11033-018-4529-5.
11. M. Ćwiklińska, M.P. Krzemiński, A. Tafelska-Kaczmarek, Chiral terpene auxiliaries III: spiroborate esters from (1R,2S,3R,5R)-3-amino-apopinan-2-ol as highly effective catalysts for asymmetric reduction of ketones with borane, Tetrahedron: Asymmetry, 26 (2015) 1453–1458. https://doi.org/10.1016/j.tetasy.2015.10.018.
12. M.U. Chopade, M.D. Nikalje, H.S. Patil, Enantioselective Formal Synthesis of the Cytotoxic Topoisomerase II Inhibitor Deoxythysanone, Catalyzed by Chiral Spiroborate Ester, Russ. J. Org. Chem. 56 (2020) 693–697. https://doi.org/10.1134/S1070428020040181.
13. F.U. Shah, S. Glavatskih, D.R. MacFarlane, A. Somers, M. Forsyth and O.N. Antzutkin, Novel halogen-free chelated orthoborate-phosphonium ionic liquids: synthesis and tribophysical properties, Phys. Chem. Chem. Phys. 13 (2011) 12865–12873. https://doi.org/10.1039/C1CP21139K.
14. F.U. Shah, A. Holmgren, M.W. Rutland, S. Glavatskih and O.N. Antzutkin, Interfacial behavior of orthoborate ionic liquids at inorganic oxide surfaces probed by nmr, ir, and raman spectroscopy, J. Phys. Chem. 122 (2018) 19687–19698. https://doi.org/10.1021/acs.jpcc.8b06049.
15. M. Taher, F.U. Shah, A. Filippov, P. De Baets, S. Glavatskih, and O.N. Antzutkin, Halogen-free pyrrolidinium bis (mandelato) borate ionic liquids: some physicochemical properties and lubrication performance as additives to polyethylene glycol, RSC Adv. 4 (2014) 30617–30623. https://doi.org/10.1039/C4RA02551B.
16. N. Hjalmarsson, E. Bergendal, Y.-L. Wang, B. Munavirov, D. Wallinder, S. Glavatskih, et al., Electro-responsive surface composition and kinetics of an ionic liquid in a polar oil. Langmuir 35 (2019) 15692–15700. https://doi.org/10.1021/acs.langmuir.9b02119.
17. P. Rohlmann, B. Munavirov, I. Furó, O. Antzutkin, S. Glavatskih and M.W. Rutland, Non-halogenated ionic liquid dramatically enhances tribological performance of biodegradable oils. Front. Chem. 7 (2019) 98. https://doi.org/10.3389/fchem.2019.00098.
18. M.V. Kazachek, I.V. Svistunova, Excited states and absorption spectra of 2-b-diketonato-1,3,2-benzodioxaborol with aromatic substituents: quantumchemistry modeling, Spectrochim. Acta A 148 (2015) 60 – 65. https://doi.org/10.1016/j.saa.2015.03.112.
19. S.N. Margar, L. Rhyman, P. Ramasami, N. Sekar, Fluorescent difluoroboron-curcumin analogs: an investigation of the electronic structures and photophysical properties, Spectrochim. Acta Part A 152

(2016) 241–251. https://doi.org/10.1016/j.saa.2015.07.064.

20. A.B. Trofimov, J. Schirmer, V.B. Kobychev, A.W. Potts, D.M.P. Holland, L. Karlsson, Photoelectron spectra of the nucleobases cytosine, thymine and adenine, J. Phys. B: At. Mol. Opt. Phys. 39 (2006) 305–326. https://doi.org/10.1088/0953-4075/39/2/007.
21. W. von Niessen, J. Schirmer, and L.S. Cederbaum, "Computational methods for the one-particle Green's function," Comp. Phys. Rep. 1 (1984) 57–125. https://doi.org/10.1016/0167-7977(84)90002-9.
22. I.S. Osmushko, V.I. Vovna, S.A. Tikhonov, Y.V. Chizhov, I.V. Krauklis, Application of DFT for the modeling of the valence region photoelectron spectra of boron and d-element complexes and macromolecules, Int. J. Quantum Chem. 116 (2016) 325–332. https://doi.org/10.1002/qua.25011.
23. U. Salzner, R. Baer, Koopmans' springs to life, J. Chem. Phys. 131 (2009) 231101. https://doi.org/10.1063/1.3269030.
24. A.D. McLachlan, M.A. Ball, Time-Dependent Hartree—Fock Theory for Molecules, *Rev. Mod. Phys.* 36 (1964) 844 – 855. https://doi.org/10.1103/RevModPhys.36.844.
25. M.E. Casida, M. Huix-Rotllant, Progress in time-dependent density-functional theory, Annu. Rev. Phys. Chem. 63 (2012) 287–323. https://doi.org/10.1146/annurev-physchem-032511-143803.
26. J. Schirmer, A. Dreuw, Critique of the foundations of time-dependent density functional theory, *Phys. Rev. A* 75 (2007) 022513 1 – 16. https://doi.org/10.1103/PhysRevA.75.022513.
27. J. Schirmer, A. Dreuw, Reply to "Comment on 'Critique of the foundations of time-dependent density functional theory' ", Phys. Rev. A *78* (2008) 056502 1 – 4. https://doi.org/10.1103/PhysRevA.78.056501.
28. M. Head-Gordon, R.J. Rico, M. Oumi, T.J. Lee, "A Doubles Correction to Electronic Excited-States from Configuration-Interaction in the Space of Single Substitutions," Chem. Phys. Lett. 219 (1994) 21–29. https://doi.org/10.1016/0009-2614(94)00070-0.
29. D. Roca-Sanjuan, F. Aquilante, R. Lindh, Multiconfiguration second-order perturbation theory approach to strong electron correlation in chemistry and photochemistry, WIREs: Comput. Mol. Sci. 2 (2012) 585–603. https://doi.org/10.1002/wcms.97.
30. B. Helmich, C. Hättig, A pair natural orbitalimplementation of the coupled cluster model CC2 for excitation energies, J. Chem. Phys. 139 (2013) 084114. https://doi.org/10.1063/1.4819071.
31. A. Dreuw, M. Wormit, The algebraic diagrammatic construction scheme for the polarization propagator for the calculation of excited state, WIREs Comput. Mol. Sci. 5 (2015) 82–95. https://doi.org/10.1002/wcms.1206.
32. C. Hättig, Structure optimizations for excited states with correlated second-order methods: CC2, CIS(D∞), and ADC(2), Adv. Quantum Chem. 50 (2005) 37–60. https://doi.org/10.1016/S0065-3276(05)50003-0.
33. P.H.P. Harbach, M. Wormit, A. Dreuw, The third-order algebraic diagrammatic construction scheme ADC(3) for the polarization propagator for closed-shell molecules: efficient implementation and benchmarking, J. Chem. Phys. 141 (2014) 064113. https://doi.org/10.1063/1.4892418.

34. R. Berraud-Pache F. Neese, G. Bistoni and R. Izsák, Unveiling the photophysical properties of boron-dipyrromethene dyes using a new accurate excited state coupled cluster method, J. Chem. Theory Comput. 16 (2019) 564–575. https://doi.org/10.1021/acs.jctc.9b00559.
35. M. Sparta, M. Retegan, P. Pinski, C. Riplinger, U. Becker, F. Neese, Multilevel Approaches within the Local Pair Natural Orbital Framework, J. Chem. Theory Comput. 13 (2017) 3198–3207. https://doi.org/10.1021/acs.jctc.7b00260.
36. S. J. Bennie, B.F.E. Curchod, F.R. Manby, D.R. Glowacki, Pushing the Limits of EOM-CCSD with Projector-Based Embedding for Excitation Energies. J. Phys. Chem. Lett. 8 (2017) 5559–5565. https://doi.org/10.1021/acs.jpclett.7b02500.
37. H.-D. Ilge, D. Fassler, H. Hartmann, Zeitschrift fur Chemie, 24 (1984) 292–293.
38. I. Bally, E. Ciornei A. Vasilescu, A. T. Balaban, Heterocyclic organoboron compounds-XVI: Chelated compounds with α, β-unsaturated β-aminoketones, Tetrahedron. 29 (1973) 3185–3187. https://doi.org/10.1016/S0040-4020(01)93464-7.
39. O. Dudek, R. H. Holm, Nuclear magnetic resonance studies of keto-enol equilibria. III. α, β-Unsaturated-β-ketoamines, J. Am. Chem. 84 (1962) 2691–2696. https://doi.org/10.1021/ja00873a009.
40. Y. P. Singh, P. Rupani, A. Singh, A. K. Rai, R. C. Mehrotra, R. D. Rogers, J. L. Atwood, Synthesis and IR, UV, NMR (1H and 11B), and mass spectral studies of new beta-ketoamine complexes of boron: crystal an molecular structure of OC6H4OBOC(R)CHC(R')NR" (R = p-ClC6H4, R' = C6H5, R" = CH3), Inorg. Chem. 25 (1986) 3076–3081. https://doi.org/10.1021/ic00237a030.
41. G.B. Guseva, E.V. Antina, A.A. Ksenofontov, E.N. Nuraneeva, A quantum chemical study of the molecular structure of zinc(II) and boron(III) complexes with monoiodo and dibromo substituted dipyrrines, J. Struct. Chem. 57 (2016) 25–32. https://doi.org/10.1134/S0022476616010042.
42. D.N. Tomilin, K.B. Petrushenko, L.N. Sobenina, M.D. Gotsko, I.A. Ushakov, A.D. Skitnevskaya, A.B. Trofimov, B.A. Trofimov, Synthesis and optical properties of meso–CF3–BODIPY with acylethynyl substituents in the 3–position of the indacene core, Asian J. Org. Chem. 5 (2016) 1288–1294. https://doi.org/10.1002/ajoc.201600303.
43. H. Zhang, C. Liu, J. Xiu, J. Qiu, Triphenylamine–modified difluoroboron dibenzoylmethane derivatives: synthesis, photophysical and electrochemical properties, Dyes Pigm. 136 (2017) 798–806 https://doi.org/10.1016/j.dyepig.2016.09.036.
44. D.A. Merkushev, S.D. Usoltsev, Yu.S. Marfin, A.P. Pushkarev, D. Volyniuk, J.V. Grazulevicius, E.V. Rumyantsev, BODIPY associates in organic matrices: spectral properties, photostability and evaluation as OLED emitters, Mater. Chem. Phys. 187 (2017) 104–111. https://doi.org/10.1016/j.matchemphys.2016.11.053.
45. Y. Bai, X. Shi, Y. Chen, C. Zhu, Y. Jiao, Z. Han, W. He, Z. Guo, Coumarin/BODIPY hybridisation for ratiometric sensing of intracellular polarity oscillation, Chem.: Eur. J. 24 (2018) 7513–7524. https://doi.org/10.1002/chem.201800915.

46. Y. Hisamune, T. Kim, K. Nishimura, M. Ishida, M. Toganoh, S. Mori, D. Kim, H. Furuta, Switch–ON near IR fluorescent dye upon protonation: helically twisted bis(boron difluoride) complex of π–extended corrorin, Chem. Eur. J. 24 (2018) 4628–4634. https://doi.org/10.1002/chem.201705516.
47. C. Lee, W. Yang, R.G. Parr, Development of the Colle-Salvetti correlation-energy formula into a functional of the electron density, Phys. Rev. B Condens. Matter Mater. Phys. 37 (1988) 785–789. https://doi.org/10.1103/PhysRevB.37.785.
48. C.J. Cramer, D.G. Truhlar, Density functional theory for transition metals and transition metal chemistry, Phys. Chem. Chem. Phys. 11 (2009) 10757–10816. https://doi.org/10.1039/B907148B.
49. S.A. Tikhonov, A.E. Sidorin, I.S. Samoilov, A.V. Borisenko, V.I. Vovna, Photoelectron spectra and electronic structure of boron diacetate formazanates, Spectrochim. Acta A Mol. Biomol. 238 (2020) 118441. 10.1016/j.saa.2020.118441.
50. T.H. Dunning, Gaussian basis sets for use in correlated molecular calculations. I. The atoms boron through neon and hydrogen, J. Chem. Phys. 90 (1989) 1007–1023. https://doi.org/10.1063/1.456153.
51. R.A. Kendall, T.H. Dunning, R.J. Harrison, Electron affinities of the first-row atoms revisited. Systematic basis sets and wave functions, J. Chem. Phys. 96 (1992) 6796–6806. https://doi.org/10.1063/1.462569.
52. M.W. Schmidt, K.K. Baldridge, J.A. Boatz, S.T. Elbert, M.S. Gordon, J.H. Jensen, S. Koseki, N. Matsunaga, K.A. Nguyen, S. Su, T.L. Windus, M. Dupuis, J.A. Montgomery, General Atomic and Molecular Electronic Structure System, J. Comput. Chem. 14 (1993) 1347–1363. https://doi.org/10.1002/jcc.540141112.
53. T. Yanai, D.P. Tew, N.C. Handy, A new hybrid exchange-correlation functional using the Coulomb-attenuating method (CAM-B3LYP), Chem. Phys. Lett. 393 (2004) 51–57. https://doi.org/10.1016/j.cplett.2004.06.011.
54. H. Thomas, Jr. Dunning, Gaussian basis sets for use in correlated molecular calculations. I. The atoms boron through neon and hydrogen, J. Chem. Phys. 90 (1989) 1007–1023. https://doi.org/10.1063/1.456153.
55. F. Neese, The ORCA program system, WIREs Comput. Mol. Sci. 2 (2012) 73–78. https://doi.org/10.1002/wcms.81.
56. Gaussian 16, Revision B.01, M.J. Frisch, G.W. Trucks, H.B. Schlegel, G.E. Scuseria, M.A. Robb, J.R. Cheeseman, G. Scalmani, V. Barone, G.A. Petersson, H. Nakatsuji, X. Li, M. Caricato, A.V. Marenich, J. Bloino, B.G. Janesko, R. Gomperts, B. Mennucci, H.P. Hratchian, J.V. Ortiz, A.F. Izmaylov, J.L. Sonnenberg, D. Williams-Young, F. Ding, F. Lipparini, F. Egidi, J. Goings, B. Peng, A. Petrone, T. Henderson, D. Ranasinghe, V.G. Zakrzewski, J. Gao, N. Rega, G. Zheng, W. Liang, M. Hada, M. Ehara, K. Toyota, R. Fukuda, J. Hasegawa, M. Ishida, T. Nakajima, Y. Honda, O. Kitao, H. Nakai, T. Vreven, K. Throssell, J. A. Montgomery, Jr., J.E. Peralta, F. Ogliaro, M.J. Bearpark, J.J. Heyd, E.N. Brothers, K.N. Kudin, V.N. Staroverov, T.A. Keith, R. Kobayashi, J. Normand, K. Raghavachari, A.P. Rendell, J.C.

Burant, S.S. Iyengar, J. Tomasi, M. Cossi, J.M. Millam, M. Klene, C. Adamo, R. Cammi, J.W. Ochterski, R.L. Martin, K. Morokuma, O. Farkas, J.B. Foresman, D.J. Fox, Gaussian, Inc., Wallingford CT, 2016.

57. V.I. Vovna, S.A. Tikhonov, I.B. Lvov, I.S. Osmushko, I.V. Svistunova, O.L. Shcheka, Photoelectron spectra an electronic structure of some spiroborate complexes, J. Electron Spectrosc. Relat. Phenom. 197 (2014), 43–49. https://doi.org/10.1016/j.elspec.2014.08.009.
58. J.J. Yeh, I. Lindau, Atomic subshell photoionization cross sections and symmetry parameters: 1 < Z < 103, At. Data Nucl. Data Tables 32 (1985). https://doi.org/10.1016/0092-640X(85)90016-6.
59. V.I. Vovna, S.A. Tikhonov, M.V. Kazachek, I.B. Lvov, V.V. Korochentsev, E.V. Fedorenko, A.G. Mirochnik, Electronic structure and optical properties of boron difluoride dibenzoylmethane F2Bdbm, J. Electron Spectrosc. Relat. Phenom. 189 (2013) 116–121. https://doi.org/10.1016/j.elspec.2013.08.009.
60. S.A. Tikhonov, V.I. Vovna, N.A. Gelfand, I.S. Osmushko, E.V. Fedorenko, A.G. Mirochnik, Electronic structure and optical properties of boron difluoride dibenzoylmethane derivatives, J. Phys. Chem. A 120 (2016) 7361–7369. https://doi.org/10.1021/acs.jpca.6b07242.
61. S. Hu¨fner, Photoelectron Spectroscopy: Principles and Applications, Springer, Berlin, 1996

Figures

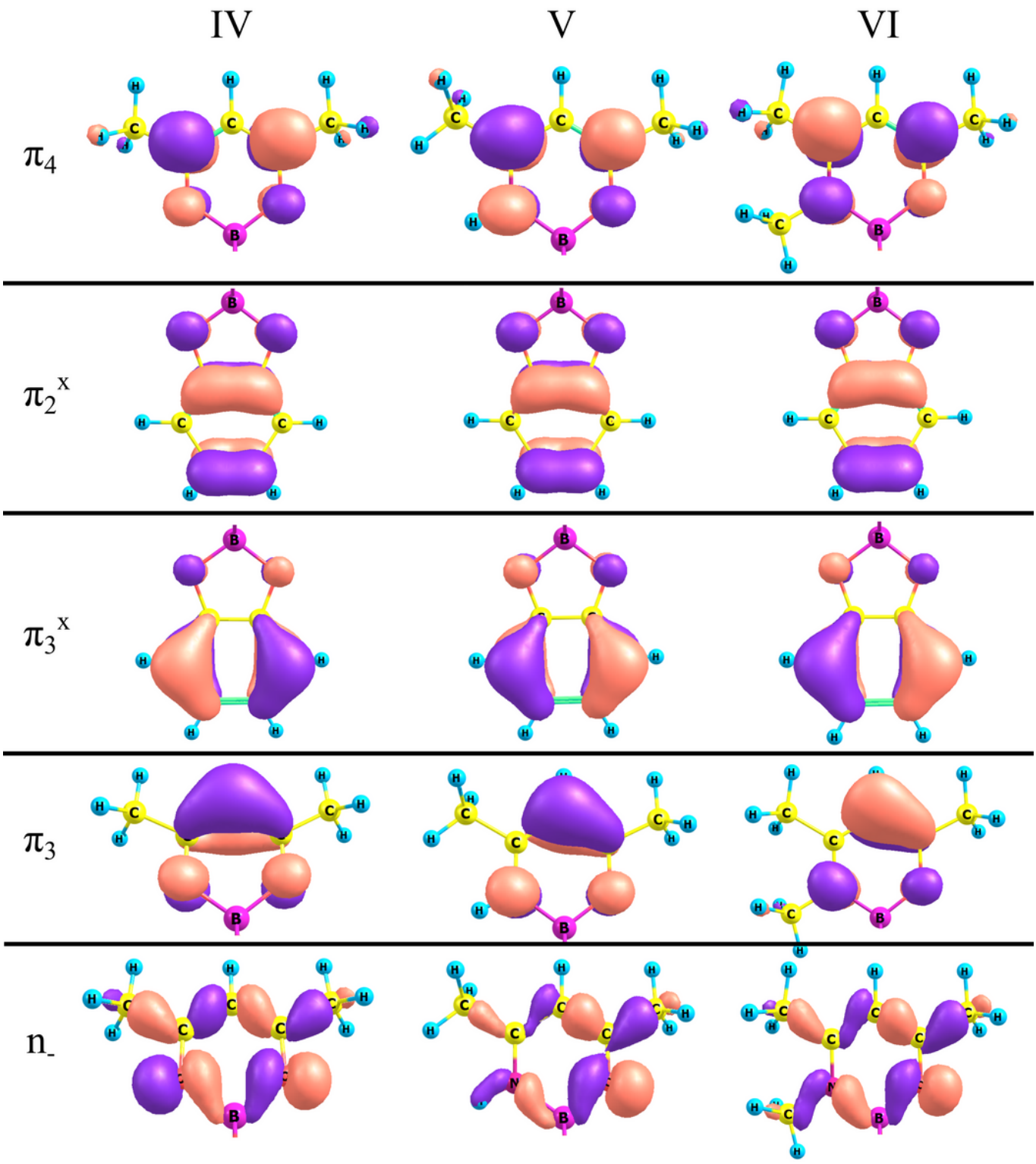


Figure 1

Some molecular orbitals of compounds IV–VI.

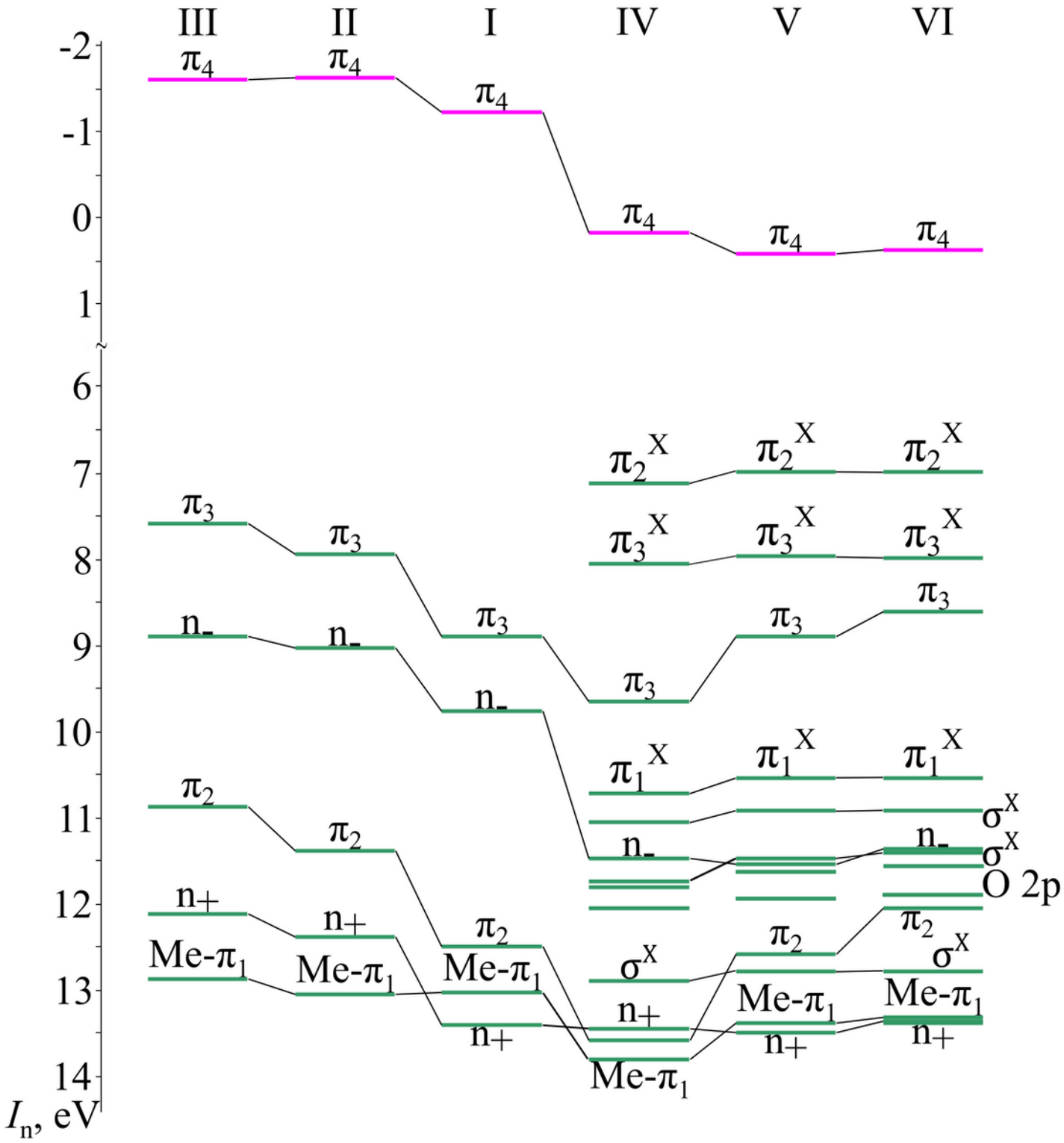


Figure 2

A diagram correlating the lower unoccupied and occupied molecular orbitals of compounds IV–VI based on the vertical ionization energies computed using the OVGF/cc-pVDZ.

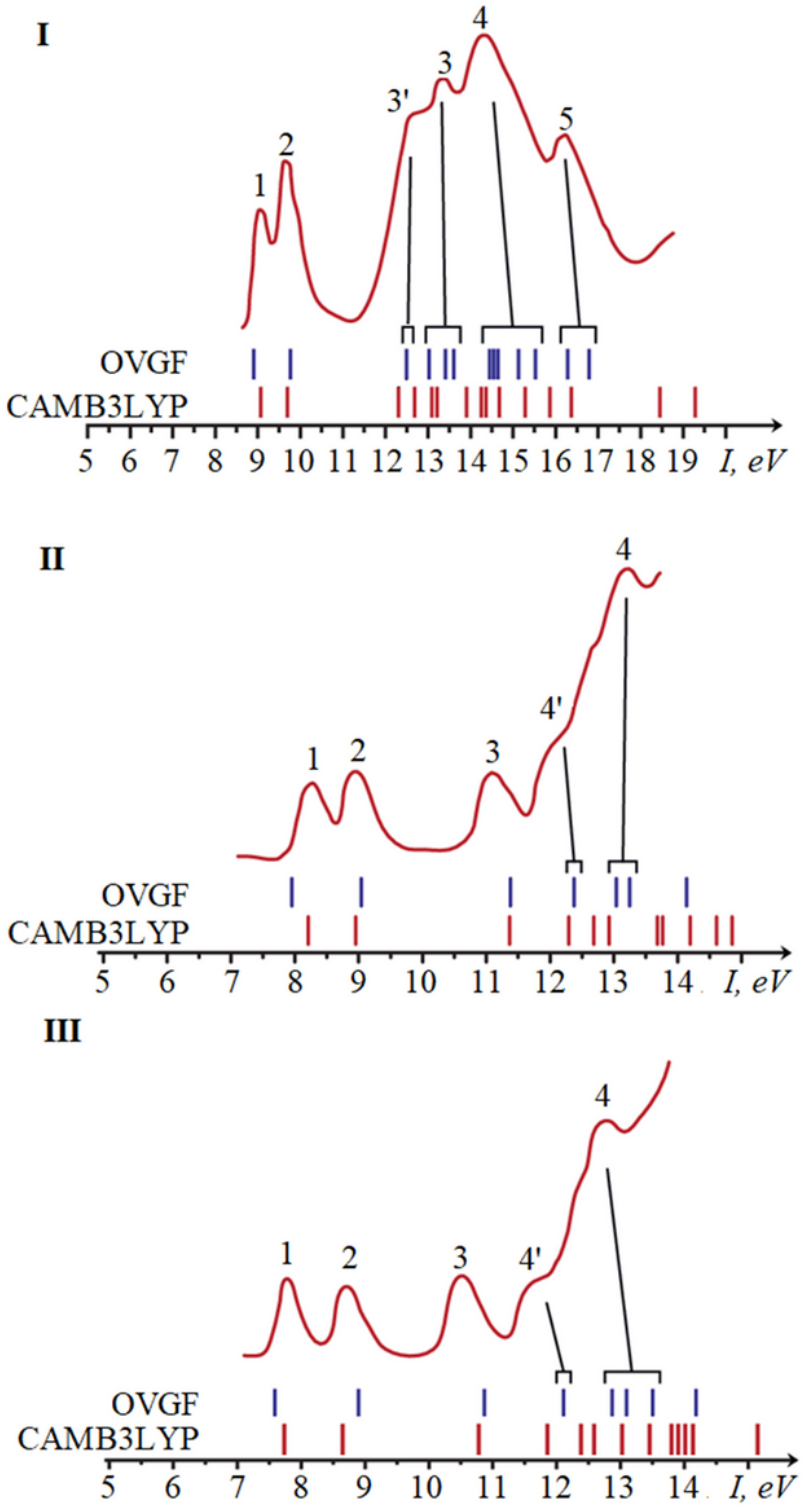


Figure 3

Ultraviolet photoelectron spectra of the vapors of compounds I–III. Colored lines correspond to calculated energies of MOs (OVGF/cc-pVDZ and DFT/CAMB3LYP/cc-pVDZ).

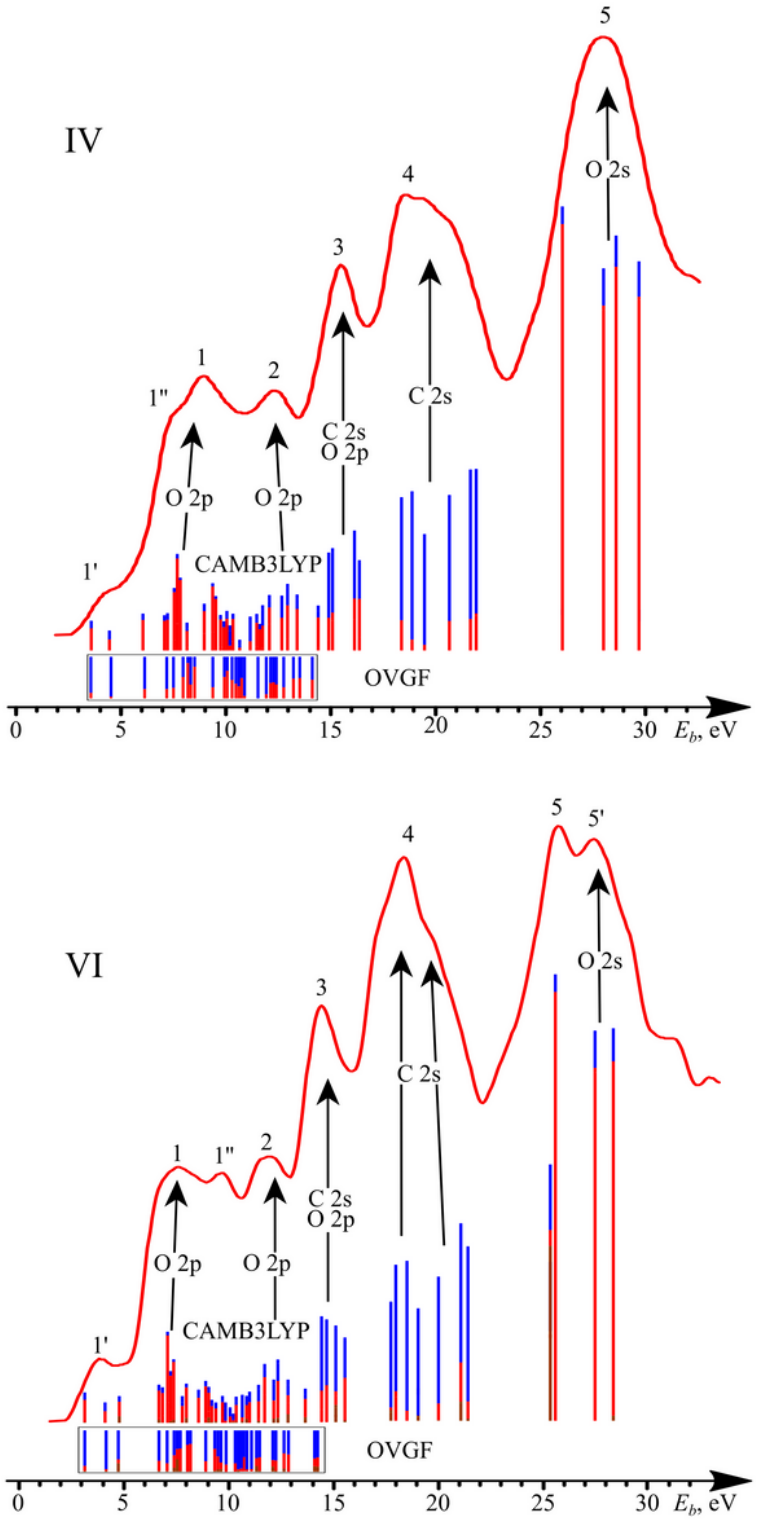


Figure 4

XPS spectrum of valence levels of compounds IV (top) and VI (bottom). Colored lines correspond to calculated energies of MOs (OVGF/cc-pVDZ and DFT/CAMB3LYP/cc-pVDZ). The line color refers to the type of atom on which the MO is localized and change as follows: carbon – blue, nitrogen – brown and oxygen – red. The height of the vertical lines corresponds to the contribution of atomic orbitals.

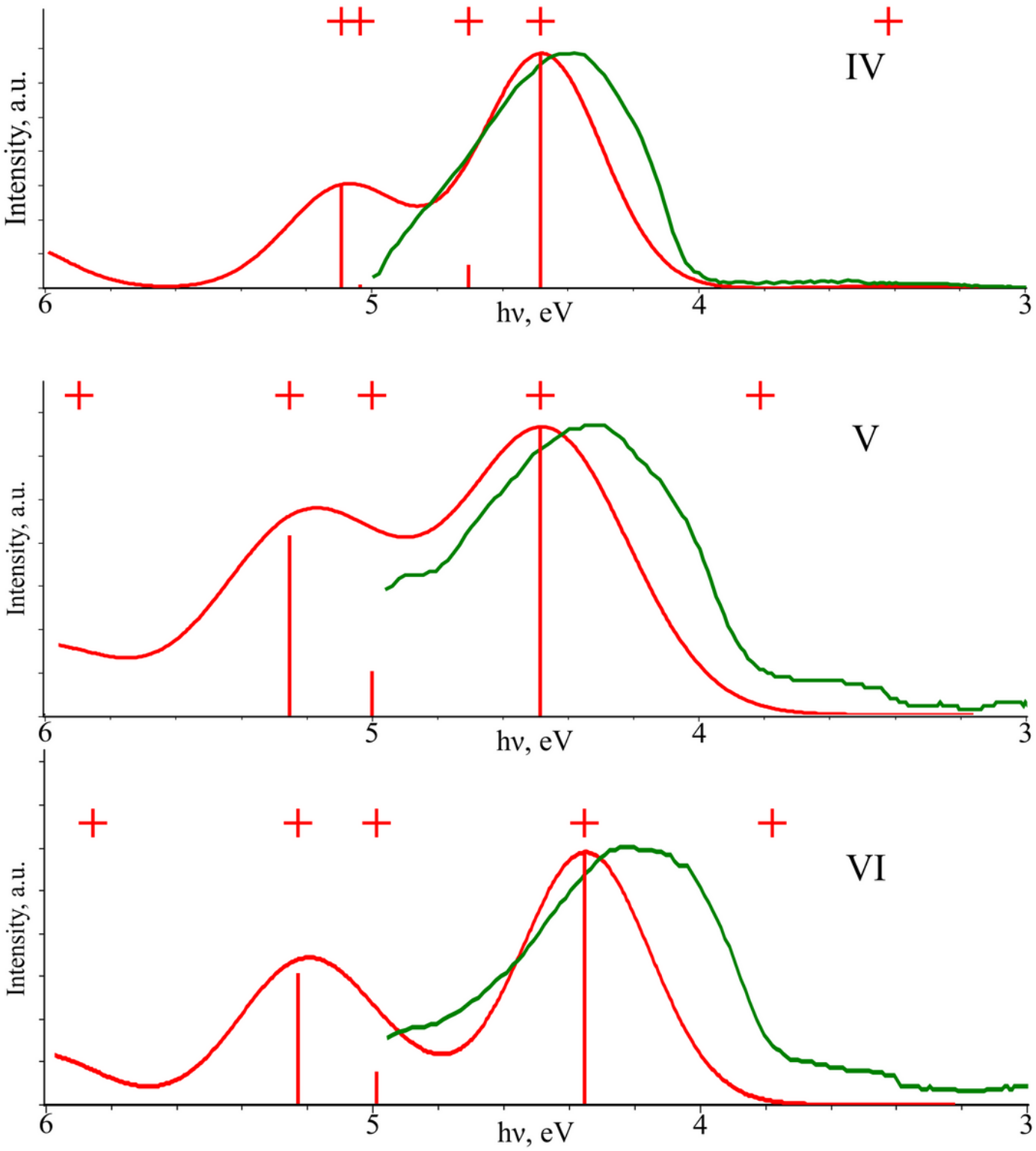


Figure 5

Optical spectra of compounds IV–VI. The experimental absorption spectra (green line) and theoretical absorption spectra are marked by the red (ADC(2)/cc-pVDZ) lines.

Supplementary Files

This is a list of supplementary files associated with this preprint. Click to download.

- SupplementaryInformation.docx